Structure and kinetic characterization of human sperm-specific glyceraldehyde-3-phosphate dehydrogenase, GAPDS

Apirat Chaikuad, Naeem Shafqat, Ruby Al-Mokhtar, Gus Cameron, Anthony R Clarke, Leo Brady, Udo Oppermann, Jan Frayne, Wyatt W. Yue

▶ **To cite this version:**

Apirat Chaikuad, Naeem Shafqat, Ruby Al-Mokhtar, Gus Cameron, Anthony R Clarke, et al.. Structure and kinetic characterization of human sperm-specific glyceraldehyde-3-phosphate dehydrogenase, GAPDS. Biochemical Journal, 2011, 435 (2), pp.401-409. 10.1042/BJ20101442 . hal-00581535

HAL Id: hal-00581535
https://hal.science/hal-00581535

Submitted on 31 Mar 2011

HAL is a multi-disciplinary open access archive for the deposit and dissemination of scientific research documents, whether they are published or not. The documents may come from teaching and research institutions in France or abroad, or from public or private research centers.

L'archive ouverte pluridisciplinaire **HAL**, est destinée au dépôt et à la diffusion de documents scientifiques de niveau recherche, publiés ou non, émanant des établissements d'enseignement et de recherche français ou étrangers, des laboratoires publics ou privés.

Biochemical Journal Immediate Publication. Published on 26 Jan 2011 as manuscript BJ20101442

Structure and kinetic characterization of human sperm-specific glyceraldehyde-3-phosphate dehydrogenase, GAPDS

Apirat Chaikuad[*1], Naeem Shafqat[*1], Ruby Al-Mokhtar[†1], Gus Cameron[†], Anthony R. Clarke[†], R. Leo Brady[†], Udo Oppermann[*‡], Jan Frayne[†2] and Wyatt W. Yue[*2]

[*] Structural Genomics Consortium
University of Oxford
Oxford, UK OX3 7DU

[†] School of Biochemistry
University of Bristol
Bristol, UK BS8 1TD

[‡] Botnar Research Centre
NIHR Biomedical Research Unit
Oxford, UK OX3 7LD

[1] These authors contribute equally to this work.
[2] Correspondence may be addressed to either of these authors (email jan.frayne@bristol.ac.uk or wyatt.yue@sgc.ox.ac.uk).

Short title: Structure and kinetics of human GAPDS

THIS IS NOT THE VERSION OF RECORD - see doi:10.1042/BJ20101442

Accepted Manuscript

Licenced copy. Copying is not permitted, except with prior permission and as allowed by law.
© 2011 The Authors Journal compilation © 2011 Portland Press Limited

Biochemical Journal Immediate Publication. Published on 26 Jan 2011 as manuscript BJ20101442

SYNOPSIS

Human sperm-specific glyceraldehyde-3-phosphate dehydrogenase (hGAPDS) is a glycolytic enzyme essential for the survival of spermatozoa, and constitutes a potential target for non-hormonal contraception. However, enzyme characterization of GAPDS has been hampered by the difficulty in producing soluble recombinant protein. Here, we have over-expressed in *E. coli* a highly-soluble form of hGAPDS truncated at the N-terminus ($hGAPDS_{\Delta N}$), and crystallized the homo-tetrameric enzyme in two ligand complexes. The $hGAPDS_{\Delta N}$-NAD^+-phosphate structure maps the two anion recognition sites within the catalytic pocket that correspond to the conserved P_s site and the newly recognised P_i site identified in other organisms. The $hGAPDS_{\Delta N}$-NAD^+-glycerol structure shows serendipitous binding of glycerol at the P_s and new P_i sites, demonstrating the propensity of these anion recognition sites to bind non-physiologically-relevant ligands. A comparison of kinetic profiles between $hGAPDS_{\Delta N}$ and its somatic equivalent reveals a moderate 3-fold increase in catalytic efficiency for $hGAPDS_{\Delta N}$. This may be attributable to subtle amino acid substitutions peripheral to the active centre that influence the charge properties and protonation states of catalytic residues. Our data therefore elucidate structural and kinetic features of hGAPDS that might provide insightful information towards inhibitor development.

Abbreviations

GAPDH, glyceroldehyde-3-phosphate dehydrogenase; GAPDS, glyceraldehyde-3-phosphate dehydrogenase, sperm-specific; G3P, glyceraldehyde-3-phosphate; PDB, protein data bank; RMSD, root-mean-square deviation.

THIS IS NOT THE VERSION OF RECORD - see doi:10.1042/BJ20101442

Accepted Manuscript

Licenced copy. Copying is not permitted, except with prior permission and as allowed by law.
© 2011 The Authors Journal compilation © 2011 Portland Press Limited

Biochemical Journal Immediate Publication. Published on 26 Jan 2011 as manuscript BJ20101442

THIS IS NOT THE VERSION OF RECORD - see doi:10.1042/BJ20101442

INTRODUCTION

The glycolytic enzyme glyceraldehyde-3-phosphate dehydrogenase (GAPDH; E.C. 1.2.1.12) catalyzes the NAD^+-dependent oxidative phosphorylation of D-glyceraldehyde-3-phosphate (D-G3P) to form 1,3-diphosphoglycerate (DPG). GAPDH is widely recognised as a drug target due to its central role in glycolysis, and in non-glycolytic processes such as nuclear RNA transport, DNA replication and repair, membrane fusion and apoptosis [1]. For example, GAPDHs from trypanosomatid species, which depend heavily on glycolysis for ATP production, are promising drug targets to combat tropical parasitic diseases [2-4]. In mammals, accumulation of GAPDH in the nucleus is linked to cell death [5], hence its inhibition might provide an anti-apoptotic application. In several neurodegenerative diseases associated with the expression of mutant poly-glutamine proteins, e.g. Huntington's disease (HD), GAPDH has been shown to bind the mutant proteins [6]. GAPDH also reportedly binds the amyloid precursor protein (APP), implying a potential role in the development of Alzheimer's disease [7].

Mammals possess not only the somatic GAPDH isozyme present in all tissues except spermatozoa, but also a sperm-specific isozyme (GAPDS) expressed at late stages of spermatogenesis [8, 9]. GAPDS shows significant sequence divergence from its somatic counterpart. For example, human GAPDS (hGAPDS) shares only 56% sequence identity with its somatic counterpart (hGAPDH; Figure S1A), and contains a unique N-terminal 72-residue polyproline extension [8] necessary for tight association with the cytoskeletal fibrous sheath of the spermatozoa flagellum [10]. The coordinated movements of sperm require substantial amounts of ATP provided by glycolysis, as evidenced by the compartmentalization of glycolytic enzymes in spermatogenic cells [11]. A *GAPDS*$^{-/-}$ knockout mouse suffered defects in sperm motility, a crucial determinant for male fertility [12], revealing the potential of targeting GAPDS as a novel contraceptive method alternative to the hormone-based approaches. Chlorinated anti-fertility compounds have been shown to inhibit sperm motility by selectively targeting the sperm-specific and not the somatic enzyme [13-15], albeit with side effects from *in vivo* trials [16, 17].

To date, the wealth of structural data from archaeal [18], bacterial [19, 20] and eukaryotic GAPDHs [21-23] have revealed a common two-domain architecture and homo-tetramer assembly. Uniform cofactor and D-G3P substrate binding pockets featuring two anion recognition sites (traditionally known as P_s and P_i sites, for the binding of substrate and inorganic phosphate respectively) have also been well documented [20, 24]. Combined with extensive kinetic studies [25, 26], the structures are consistent with a well-accepted flip-flop reaction mechanism. This begins with a nucleophilic attack by a cysteine sulfhydryl on the carbonyl of D-G3P to form a thio-hemiacetal intermediate followed by hydride transfer from the thio-hemiacetal to NAD^+. The resulting thioacyl-enzyme is then attacked by an inorganic phosphate to form DPG. In this model, the C3 phosphate of substrate D-G3P is expected to bind to the P_i site during the formation of the hemiacetal intermediate, and flips to the P_s site before hydride transfer, to vacate the P_i site for an incoming inorganic phosphate [20, 27].

Compared to somatic GAPDHs which have been structurally and kinetically characterized (reviewed in [28]), the sperm-specific isozyme GAPDS has proven intractable to study largely due to the insolubility of native and recombinant proteins. Recently, the structure of a hetero-tetrameric complex of rat GAPDS-*E. coli* GAPDH has been reported to moderate resolution, [29], and provided the first view of a mammalian GAPDS, albeit within an unnatural oligomer. Here, we have over-expressed human GAPDS truncated at the N-terminus ($hGAPDS_{\Delta N}$), to gain insights into its structural and kinetic properties. The $hGAPDS_{\Delta N}$ homo-tetrameric crystal structures, determined in complexes with phosphate and NAD^+ ($hGAPDS_{\Delta N}$-NAD^+-PO_4) and with glycerol and NAD^+ ($hGAPDS_{\Delta N}$-NAD^+-Gol), provide the first high-

Licenced copy. Copying is not permitted, except with prior permission and as allowed by law.
© 2011 The Authors Journal compilation © 2011 Portland Press Limited

Accepted Manuscript

Biochemical Journal Immediate Publication. Published on 26 Jan 2011 as manuscript BJ20101442

resolution view of the two anion recognition sites in a human enzyme. Combined with a comparative kinetic analysis, these structures provide a rigorous description of the sperm-specific isozyme that may assist inhibitor design.

Accepted Manuscript

THIS IS NOT THE VERSION OF RECORD - see doi:10.1042/BJ20101442

Licenced copy. Copying is not permitted, except with prior permission and as allowed by law.
© 2011 The Authors Journal compilation © 2011 Portland Press Limited

Biochemical Journal Immediate Publication. Published on 26 Jan 2011 as manuscript BJ20101442

EXPERIMENTAL

Protein expression and purification

A DNA fragment encoding hGAPDS (hGAPDS$_{\Delta N}$, aa 69-398; GenBank entry 7657116) was subcloned into the pNIC-CTHF vector (GenBank entry 124015079) incorporating a C-terminal TEV-cleavable His$_6$-tag. The corresponding plasmid was transformed into *Escherichia coli* BL21(DE3)-R3, cultured in 1 L of Terrific Broth at 37 °C, and induced with 0.5 mM IPTG overnight at 18 °C. Cells were homogenized in lysis buffer (50 mM HEPES pH 7.5, 500 mM NaCl, 5% (*v*/*v*) glycerol, 20 mM imidazole) and insoluble material was removed by centrifugation. The supernatant was purified by affinity (Ni-sepharose) and size-exclusion (Superdex S75) chromatography. Purified protein was treated with His-tagged TEV protease overnight at 4 °C, and then passed over 1 mL of Ni-Sepharose resin. The TEV-treated protein, containing the remnant vector-encoded sequence 'AENLYFQ' at the C-terminus, was concentrated to 12 mg/ml and stored in storage buffer (10 mM HEPES pH 7.5, 500 mM NaCl, 5% (*v*/*v*) glycerol, 0.5 mM tris(2-carboxyethyl)phosphine hydrochloride (TCEP) at -80 °C.

Crystallization and data collection

hGAPDS$_{\Delta N}$ was crystallized at 4 °C in 150-nl drops using the sitting drop vapour diffusion method. Viable crystals of the hGAPDS$_{\Delta N}$-NAD$^+$-PO$_4$ complex were obtained by mixing protein pre-incubated with 5mM NAD$^+$ (Sigma) with the reservoir solution (20% PEG 3350, 0.2 M Na/K phosphate and 10% (*v*/*v*) ethylene glycol) in a 1:2 volume ratio. Crystals of the hGAPDS$_{\Delta N}$-NAD$^+$-Gol complex were fortuitously obtained from mixing protein alone with reservoir solution (20% PEG 3350, 0.2 M Na_2SO_4, 10% (*v*/*v*) ethylene glycol and 0.1 M bis-tris propane pH 6.5) in a 1:1 volume ratio. Attempts to crystalize hGAPDS$_{\Delta N}$ in the *apo* form have not been successful to date. All crystals were cryo-protected with reservoir solution supplemented with 25% (v/*v*) glycerol, and flash-cooled in liquid nitrogen. Diffraction data were collected on beamline I03 at the Diamond Light Source (hGAPDS$_{\Delta N}$-NAD$^+$-PO$_4$) and in-house on a Rigaku FR-E Superbright source (hGAPDS$_{\Delta N}$-NAD$^+$-Gol). Data were processed with MOSFLM and SCALA from the CCP4 Suite [30].

Structure determination

Both crystal forms belong to the C-centered monoclinic spacegroup *C*2 (Table 1). Structures were solved by molecular replacement with PHASER [31] using the rat sperm GAPDS coordinates [29] as a search model. Density modification and NCS averaging were performed with DM [32], and the improved phases were used for automated model building with Buccaneer [33]. Iterative cycles of manual model building using COOT [34] alternated with refinement in REFMAC5 [35] were performed. At the last refinement step TLS restrained refinement was applied using TLS tensor groups determined by the TLSMD server [36]. Data collection and refinement statistics are summarised in Table 1.

Steady-state enzyme kinetics

Recombinant hGAPDS$_{\Delta N}$ was dialyzed against storage buffer containing activated charcoal to remove bound cofactor, enabling accurate measurement of protein concentration. Examination of the protein spectra showed no NAD$^+$ absorbance at 260 nm showing that the NAD$^+$ had been successfully removed. Kinetic assays were based on the forward reaction, in which phosphorylation of D-G3P was catalyzed in the presence of NAD$^+$ and inorganic phosphate [37]. All reactions were performed in 10 mM sodium pyrophosphate, 20 mM sodium phosphate pH 8.5, 3 µM dithiothreitol and 10 mM sodium arsenate, using 500 ng/ml enzyme. The K_M for D-G3P was measured using concentration range 0.3-4.0 mM at a fixed NAD$^+$ concentration (0.5 mM). The K_M for NAD$^+$ was determined using concentration range 0.02-1 mM at a fixed D-G3P concentration (1.5 mM). All reagents apart from hGAPDS$_{\Delta N}$ were dispensed in a 96-

THIS IS NOT THE VERSION OF RECORD - see doi:10.1042/BJ20101442

Accepted Manuscript

Licenced copy. Copying is not permitted, except with prior permission and as allowed by law.
© 2011 The Authors Journal compilation © 2011 Portland Press Limited

Biochemical Journal Immediate Publication. Published on 26 Jan 2011 as manuscript BJ20101442

well plate, and pre-incubated at 25 °C for 2 min. The reaction was initiated by the addition of $hGAPDS_{\Delta N}$. Steady-state reactions were recorded at 340 nm for 3 min with readings taken every 2 sec, using a VERSAmax microplate reader (Molecular Devices Corp, UK). The tangent at time zero was well defined and accurately defined the initial velocity. Values for K_M, V_{max} and k_{cat} were calculated using GraphPad Prism (GraphPad Software Inc.) by non-linear regression analysis. The same process and parallel kinetic assays were also performed with human GAPDH from erythrocytes (Sigma).

Accession numbers

Atomic coordinates and structure factors have been deposited in the Protein Data Bank under the accession numbers 3h9e ($hGAPDS_{\Delta N}$-NAD^+-PO_4) and 3pfw ($hGAPDS_{\Delta N}$-NAD^+-Gol).

THIS IS NOT THE VERSION OF RECORD - see doi:10.1042/BJ20101442

Accepted Manuscript

Licenced copy. Copying is not permitted, except with prior permission and as allowed by law.
© 2011 The Authors Journal compilation © 2011 Portland Press Limited

Biochemical Journal Immediate Publication. Published on 26 Jan 2011 as manuscript BJ20101442

THIS IS NOT THE VERSION OF RECORD - see doi:10.1042/BJ20101442

RESULTS

Recombinant production and structure determination of hGAPDS$_{\Delta N}$

To identify the optimal domain boundary of hGAPDS for structural studies, we expressed a series of full-length and truncated constructs in *E. coli* as N/C-terminally His-tagged proteins (Figure S1B). We observed that the full-length protein was predominantly insoluble when recombinantly expressed. High levels of soluble expression were found in several N-terminally truncated constructs harbouring the His-tag at the C-terminus, while fusing the affinity tag to the N-terminus of the equivalent constructs render them less soluble. We subsequently purified the C-terminal His-tagged construct encompassing aa 69-407 (referred hereafter as hGAPDS$_{\Delta N}$) to homogeneity (Figure S1C) and its crystal structure was determined in two complexes: one bound with NAD^+ and inorganic phosphate (hGAPDS$_{\Delta N}$-NAD^+-PO_4) at 1.72 Å resolution, and the other bound with NAD^+ and glycerol (hGAPDS$_{\Delta N}$-NAD^+-Gol) at 2.15 Å resolution (Table 1).

In both hGAPDS$_{\Delta N}$ complexes, the asymmetric unit comprises two subunits *O* and *P* (C_α-RMSD between subunits ~0.1-0.2 Å) (Figure 1A), which generate another subunit pair *Q* and *R* by a twofold symmetry operation (lying approximately on the *RQ* plane, using previous nomenclature [38]), resulting in a homotetramer with 222 point symmetry (Figure 1B). Similar to other GAPDHs, each subunit consists of an N-terminal nucleotide binding domain (N-domain; aa 69-220) and a C-terminal catalytic domain (C-domain; aa 223-407). The N-domain consists of an eight-stranded β-core flanked by helices on both sides in a classical Rossmann fold. The C-domain is built from a five-stranded β-sheet core with helices on one side, and harbours the active-site catalytic residues Cys224 and His251, as well as a conserved S-shaped loop (S-loop; aa 252-278) that forms the tetrameric core. The S-loop constitutes the main site of intersubunit contacts and has previously been suggested to determine NAD/NADP cofactor specificity [39]. The hGAPDS$_{\Delta N}$ structures are similar to other GAPDHs e.g. human liver/placental (hGAPDH) [22], *Bacillus sterothermophilus* (*Bs*GAPDH) [20, 27, 40], *E. coli* (*Ec*GAPDH) [19] and *Leishmania mexicana* (*Lm*GAPDH) [2-4] enzymes, as evidenced by C_α-RMSD values ranging from 0.7-2.3 Å albeit sharing only 20-67% sequence identity.

The hGAPDS$_{\Delta N}$ homo-tetramer

The quaternary arrangement and intersubunit interfaces of hGAPDS$_{\Delta N}$ are consistent with the functional oligomeric state proposed for other GAPDHs, with subtle differences in two features namely the electrostatic surface potential and intersubunit selectivity cleft. The hGAPDS$_{\Delta N}$ structures reveal three prominently charged patches at the dimeric and tetrameric interfaces, contributed from the positively-charged S-loop (aa 252-278), the negatively-charged 350-372 region and the mix-charged 106-130 region (Figure 1C). The widespread charge distribution in hGAPDS$_{\Delta N}$ is more prominent than somatic hGAPDH (PDB id 1u8f, 1znq) due to several non-conserved charged/polar residues (e.g. Glu112, Lys119, Tyr127, Lys128, Ser252, Tyr253, Arg265, His275, Asp351, Glu352, Lys370) (Figure S1A), and suggests that hGAPDS$_{\Delta N}$ tetramerization is facilitated via intersubunit electrostatic complementarity. For example, at the dimeric interface the positively-charged S-loop of subunit *P* protrudes into a negatively-charged groove from the 350-372 region of subunit *O*, creating a number of salt bridges (Figure S2). At the tetrameric interface, close to the cofactor binding site, the mix-charged 106-130 region of subunit *O* packs against the positively-charged S-loop of subunit *R* and the negatively-charged 350-372 region of subunit *Q*

A second differentiating feature between hGAPDH and hGAPDS$_{\Delta N}$ is the selectivity cleft adjacent to the adenosine pocket of the NAD^+-binding site (Figure 1D). The selectivity cleft exhibits cross-species

Accepted Manuscript

Licenced copy. Copying is not permitted, except with prior permission and as allowed by law.
© 2011 The Authors Journal compilation © 2011 Portland Press Limited

Biochemical Journal Immediate Publication. Published on 26 Jan 2011 as manuscript BJ20101442

THIS IS NOT THE VERSION OF RECORD - see doi:10.1042/BJ20101442

variability in size, and has been exploited for small-molecule inhibitor development as exemplified by the selective binding of an adenosine derivative NMDBA [N^6-(1-naphthalenemethyl)-2′-deoxy-2′-(3,5-dimethoxybenzamido)adenosine] to the selectivity cleft of the trypanosomatid *Lm*GAPDH (PDB id 1i32) [2-4]. In our hGAPDS$_{\Delta N}$ structures, loop β_2-α_3 residues (Phe108, Ile109 and Asp110) from one subunit (e.g. *O*) form one side of the selectivity cleft, while S-loop residues (Pro263, Ser264, Arg265 and Lys266) of another subunit (e.g. *R*) form the other side (Figure 1D). These residues are conserved between hGAPDH and hGAPDS with the exception of Arg265 in hGAPDS (Gly in hGAPDH) (Figure S1A). This Arg residue confers reduced conformational flexibility to the S-loop compared to the more adaptable glycine in hGAPDH. As a result, while the hGAPDH S-loop adopts two flexible conformations (resulting in 'open' and 'closed' states of the cleft; PDB id 1u8f, 1znq) proposed to be inherent to the somatic isozyme [22, 23], only the 'closed' state is observed in our hGAPDS$_{\Delta N}$ selectivity cleft. Furthermore, the Arg265 side-chain forms electrostatic interactions and water-mediated hydrogen bonds with Asp110 on the opposite side of the cleft, thereby constricting the cleft cavity to ~4 Å in width, compared with ~5 Å in hGAPDH [23] and 7-8 Å in *Lm*GAPDH [2, 3]. Modelling the NMDBA ligand onto the NAD^+ molecule in our structure reveals severe steric clashes with Pro263 from S-loop and Phe108 from β_2-α_3 loop (Figure 1E). This, together with a much reduced selectivity cleft cavity compared to *Lm*GAPDH, might prevent the binding of NMDBA to hGAPDS$_{\Delta N}$.

Conservation of anion binding sites in the hGAPDS$_{\Delta N}$-NAD^+-PO_4 complex

Our hGAPDS$_{\Delta N}$ complexes reveal an NAD^+ molecule bound in each subunit (Figure 2A), adopting essentially identical conformation and interactions as the rat GAPDS and somatic hGAPDH structures. Additional electron density was observed in the substrate binding pocket adjacent to the cofactor-binding site (Figure 2A) and was refined as two bound phosphate ions per subunit, presumably originating from the crystallization buffer. The positions of the two phosphate ions are identical in both subunits, and map two anion binding sites in hGAPDS that are commonly observed in other GAPDHs (Figure 2B). The first phosphate site, known previously as the P_s site, is adjacent to the nicotinamide and ribose moieties of NAD^+. The bound phosphate interacts with residues enclosing the P_s site (Thr254, Thr256, Arg306) as well as the nicotinamide ribose hydroxyl group of NAD^+ (Figure 2C, *left* panel). The second phosphate site is close to the catalytic residue Cys224 (closest phosphate oxygen is ~3.3 Å from the cysteine thiol) (Figure 2C, *right* panel) and corresponds to the 'new P_i site' previously observed in the *Lm*GAPDH (PDB id 1gyp) and *Ec*GAPDH structures (PDB id 1dc4) [19, 24]. This is at a distance of 2.5-3.0 Å from the 'original P_i site' reported for the *Bs*GAPDH structure (PDB id 1gd1) [20] which is further away from Cys224.

The two disparate P_i locations observed in various GAPDH structures are proposed to be commensurate with the two different conformations of a nearby β-loop-α segment (referred hereafter as the active site segment) - namely an 'out' conformation for the 'original P_i site' and an 'in' conformation for the 'new P_i site' (Figure 2B) [27]. In the hGAPDS$_{\Delta N}$-NAD^+-PO_4 structure, the active site segment (aa 280-292) adopts the 'in' conformation for subunit *O*, and a mixed 'in'-'out' conformation (50% occupancy each) for subunit *P* (Figure 2D). The two conformers differ structurally in the orientation of the conserved residues Thr283 and Gly284, which are displaced from the 'in' (closer to the second phosphate) to the 'out' (away from the second phosphate) conformations by ~ 2.0-3.8 Å (C_α-RMSD). Interestingly, the second phosphate from both subunits occupy the 'new P_i site' (despite presence of the 'out'-conformer in subunit *P*), and are anchored by Ser223, Thr225 and His251 (Figure 2C, *right* panel). The 'in'-conformer of subunits *O* and *P* further contributes hydrogen bonds to the second phosphate ion via the main-chain Thr283 and Gly284 atoms (~2.5-2.7 Å), which are not provided in the subunit *P* 'out'-conformer as the two residues are more distant from the second phosphate (3.7 and 5.7 Å respectively) (Figure 2D, compare *left* and *right*).

Accepted Manuscript

Licenced copy. Copying is not permitted, except with prior permission and as allowed by law.
© 2011 The Authors Journal compilation © 2011 Portland Press Limited

Biochemical Journal Immediate Publication. Published on 26 Jan 2011 as manuscript BJ20101442

Binding of glycerol in the anion recognition sites

Structural characterization of a hGAPDS$_{\Delta N}$-NAD$^+$ crystal grown in a sulphate-containing condition reveals electron density peaks at the two anion binding sites (Figure 3A) that do not fit the shape of sulphate ions often observed to bind in various GAPDH structures. Instead, this density is a good match to glycerol present in our purification and cryo-protectant buffers. As a result two glycerol molecules were refined into the P_s and 'new P_i' sites of each subunit, and we referred to this structure as the hGAPDS$_{\Delta N}$-NAD$^+$-Gol complex. Neither of the two glycerol molecules overlaps with the expected location of the substrate D-G3P glyceraldehyde moiety between the two anion recognition sites (Figure 3A). The interactions between the two glycerol molecules and the enzyme are similar to the phosphate ions from the hGAPDS$_{\Delta N}$-NAD$^+$-PO_4 structure, albeit less extensive than the phosphate ions as reflected by a degree of structural degeneracy and flexibity in the binding conformation of glycerol. Although in this structure the active site segment adopts fully the 'out' conformation, the glycerol at the new P_i site is further away from the catalytic cysteine (compared to the phosphate in the hGAPDS$_{\Delta N}$-NAD$^+$-PO_4 complex) enabling it to form direct and water-mediated polar interactions with residues from the active site segment (Ser282, Thr283 and Gly284) (Figure 3B). The water-mediated hydrogen bond network bridging the two glycerol molecules is also conserved in the hGAPDS$_{\Delta N}$-NAD$^+$-PO_4 structure.

Comparative kinetic analysis of hGAPDS$_{\Delta N}$

The steady-state kinetic properties of hGAPDS$_{\Delta N}$ were measured and compared with those of somatic hGAPDH (Table 2). The two isozymes share similar K_M values for D-G3P substrate and rate constant. However, hGAPDS$_{\Delta N}$ has a 3-fold lower K_M for NAD$^+$ (35 μM) than hGAPDH (100 μM), hence resulting in an approximately 3-fold increased catalytic efficiency (k_{cat}/K_M) with regards to NAD$^+$. The steady-state kinetics for hGAPDH in this study are comparable to those previously reported for hGAPDH purified from brain tissue [28], showing a k_{cat} of ~100 s^{-1} and K_M of 0.07 mM and 0.16 mM for NAD$^+$ and D-G3P, respectively.

THIS IS NOT THE VERSION OF RECORD - see doi:10.1042/BJ20101442

Accepted Manuscript

Licenced copy. Copying is not permitted, except with prior permission and as allowed by law.
© 2011 The Authors Journal compilation © 2011 Portland Press Limited

Biochemical Journal Immediate Publication. Published on 26 Jan 2011 as manuscript BJ20101442

THIS IS NOT THE VERSION OF RECORD - see doi:10.1042/BJ20101442

DISCUSSION

hGAPDS shares conserved structural features with other GAPDHs

Here we report the first detailed structural and kinetic characterization of human sperm-specific GAPDS. By fusing a C-terminal affinity tag and truncating the N-terminal polyproline region that hinders correct protein folding as shown in this work, and in a recent report [41], we have obtained high levels of recombinant soluble hGAPDS$_{\Delta N}$. Our work significantly extends a recent structural study on rat GAPDS [29], where very low recombinant expression levels and solubility required complexation with native *E. coli* GAPDH for crystallisation. Cross-species hetero-tetramers in various stoichiometries have been reported between GAPDH and GAPDS subunits previously [29, 42]. Nevertheless, given the proximity of the active site cleft to the subunit interfaces, it is unlikely that studies of GAPDS in these unnatural hetero-tetrameric forms provide a realistic assessment of GAPDS structure and activity. Our high-resolution hGAPDS$_{\Delta N}$ structures confirm homo-tetrameric formation and shows that electrostatic interactions and charge complementarity appear to play a substantial role in tetrameric assembly, more so than in hGAPDH, to facilitate the correct orientation of subunits. Our structures also reveal an effectively closed selectivity cleft in hGAPDS as compared to other GAPDHs, particularly the trypanosomal enzymes, and therefore lend further support to the strategy of designing species-specific inhibitors that fill the trypanosomal selectivity cleft without inhibiting the human enzymes [2, 3].

Mapping of anion recognition sites in hGAPDS

The binding positions of phosphate in our hGAPDS$_{\Delta N}$ -NAD$^+$-PO$_4$ complex map the two anion recognition sites in hGAPDS, which are occupied by glycerol in our hGAPDS$_{\Delta N}$ -NAD$^+$-Gol structure. In addition, the trapping of active-site glycerol was not unprecedented for GAPDHs, since glycerol binding to the P_s site was previously reported in an inhibitor-bound *T. cruzii* GAPDH structure (PDB id 3dmt). It remains to be determined how glycerol, presumably derived from our purification or cryo-protection buffers, out-competes the binding of sulphate ions (closely similar to the physiological phosphates) that are present in high concentration in the crystallization solution. Our findings nevertheless reveal the flexible nature and capacity of the anion recognition sites to accommodate uncharged, polar and non-physiologically relevant ligands, and provide important information to their mode of interactions.

Previous structural characterization of GAPDHs structures has led to the widely-discussed P_s and P_i nomenclature and flip-flop mechanism [19, 27, 40]. In contrast to the P_s site, the true position of the P_i site remains unclear since the identification of a 'new P_i' site (at a distance from the 'original' P_i site) in a number of GAPDH structures. The divergence in the location and number of P_i site(s) is postulated to correlate with the conformations of the neighbouring 'active site segment' alternating during catalysis, to maintain interactions between the phosphate ion and the conserved threonine and glycine residues from the active site segment (Thr283 and Gly284 in hGAPDS) [27]. The hGAPDS$_{\Delta N}$-NAD$^+$-PO$_4$ structure clearly indicates that a phosphate ion is bound at the new P_i site when the active site segment adopts the fully 'in' conformation (presumably mimicking a ternary state of enzyme poised for catalysis) and the partially 'out' conformation (presumably allowing flipping of the hemi-acetal intermediate), while we did not observe phosphate binding at the 'original' P_i site. This contrasts with the *Bs*GAPDH ternary complex, known to have both new and original P_i sites competent and partially occupied by two phosphate moieties, with the active site segment adopting two conformations [27]. It is not clear whether co-existence of two alternative P_i positions portrays a common catalytic property or a species-specific feature [27]. Since this is not the case in hGAPDS, a different mechanism for the human enzymes can be envisaged where the original P_i site may not be present.

Accepted Manuscript

Licenced copy. Copying is not permitted, except with prior permission and as allowed by law.
© 2011 The Authors Journal compilation © 2011 Portland Press Limited

Biochemical Journal Immediate Publication. Published on 26 Jan 2011 as manuscript BJ20101442

Kinetic differences between hGAPDS and hGAPDH may arise from electrostatic properties

Disregarding the unique polyproline N-terminus in hGAPDS, the amino acid differences between hGAPDS and hGAPDH are mostly confined to the protein surface, contributing to differences in their surface electrostatic potentials. The active site architecture, ligand binding mode and catalytic residues, however, are highly conserved among the isozymes, in part reflected by their kinetic parameters being in the same order of magnitude. Nevertheless, subtle differences above standard deviations are notable, particularly the moderate 3-fold higher catalytic efficiency for hGAPDS than hGAPDH. This may be attributable to the effect of amino acid substitutions peripheral to the catalytic centre, often known as '2nd sphere' residues for enzymes known to have identical active sites but different enzymatic properties [43, 44]. A number of amino acid positions lining the adenine and nicotinamide pockets of the NAD^+-binding site (Figure 4) involve point charge changes between hGAPDS and hGAPDH. For example, Tyr173 and Asp311 in hGAPDS are substituted by Phe and Asn respectively in hGAPDH (Figure 4). These '2nd sphere residues, while not perturbing the structural integrity of the active site, could influence the catalytic efficiency of the enzyme by possibly removing a hydrogen bond with NAD^+ (Tyr173Phe substitution) or by altering the pK_a and consequently the protonation state (Asp311Asn substitution) of nearby catalytic residues.

To conclude, isoform-specific inhibitor development for hGAPDS has been implemented for several decades as a strategy for non-hormonal contraception, though suffers from a lack of ligand-bound structural information for the human GAPDH isozymes. Our data highlight subtle yet significant differences in the structural and kinetic features between hGAPDS and other GAPDH enzymes, and therefore need to be considered for future design of inhibitors targeting the sperm-specific isozyme.

ACKNOWLEDGEMENTS

We thank Georgina Berridge and Rod Chalk for assistance in mass spectrometry analyses, and staff at the Diamond Light Source for access to synchrotron data collection facilities.

AUTHOR CONTRIBUTION

AC, NS performed the structural determination. RA, JF, GC, ARC, RLB performed the kinetic experiments and analyzed the data. WWY, UO, JF, RLB supervised the project. AC, WWY designed the experiments and wrote the manuscript. All authors read and approved the final manuscript.

FUNDING

The Structural Genomics Consortium is a registered charity (number 1097737) that receives funds from the Canadian Institutes for Health Research, the Canadian Foundation for Innovation, Genome Canada through the Ontario Genomics Institute, GlaxoSmithKline, Karolinska Institutet, the Knut and Alice Wallenberg Foundation, the Ontario Innovation Trust, the Ontario Ministry for Research and Innovation, Merck & Co., Inc., the Novartis Research Foundation, the Swedish Agency for Innovation Systems, the Swedish Foundation for Strategic Research and the Wellcome Trust. The work was also supported by the NIHR Biomedical Research Unit to UO, and by the Wellcome Trust (Ref: 07746) and UK BBSRC (Ref: BB/F007256) to RLB.

THIS IS NOT THE VERSION OF RECORD - see doi:10.1042/BJ20101442

Accepted Manuscript

Licenced copy. Copying is not permitted, except with prior permission and as allowed by law.
© 2011 The Authors Journal compilation © 2011 Portland Press Limited

Biochemical Journal Immediate Publication. Published on 26 Jan 2011 as manuscript BJ20101442

REFERENCES

1 Sirover, M. A. (2005) New nuclear functions of the glycolytic protein, glyceraldehyde-3-phosphate dehydrogenase, in mammalian cells. J. Cell. Biochem. **95**, 45-52

2 Aronov, A. M., Suresh, S., Buckner, F. S., Van Voorhis, W. C., Verlinde, C. L., Opperdoes, F. R., Hol, W. G. and Gelb, M. H. (1999) Structure-based design of submicromolar, biologically active inhibitors of trypanosomatid glyceraldehyde-3-phosphate dehydrogenase. Proc. Natl. Acad. Sci. U. S. A. **96**, 4273-4278

3 Suresh, S., Bressi, J. C., Kennedy, K. J., Verlinde, C. L., Gelb, M. H. and Hol, W. G. (2001) Conformational changes in Leishmania mexicana glyceraldehyde-3-phosphate dehydrogenase induced by designed inhibitors. J. Mol. Biol. **309**, 423-435

4 Aronov, A. M., Verlinde, C. L., Hol, W. G. and Gelb, M. H. (1998) Selective tight binding inhibitors of trypanosomal glyceraldehyde-3-phosphate dehydrogenase via structure-based drug design. J. Med. Chem. **41**, 4790-4799

5 Ishitani, R., Tanaka, M., Sunaga, K., Katsube, N. and Chuang, D. M. (1998) Nuclear localization of overexpressed glyceraldehyde-3-phosphate dehydrogenase in cultured cerebellar neurons undergoing apoptosis. Mol. Pharmacol. **53**, 701-707

6 Burke, J. R., Enghild, J. J., Martin, M. E., Jou, Y. S., Myers, R. M., Roses, A. D., Vance, J. M. and Strittmatter, W. J. (1996) Huntingtin and DRPLA proteins selectively interact with the enzyme GAPDH. Nat. Med. **2**, 347-350

7 Schulze, H., Schuler, A., Stuber, D., Dobeli, H., Langen, H. and Huber, G. (1993) Rat brain glyceraldehyde-3-phosphate dehydrogenase interacts with the recombinant cytoplasmic domain of Alzheimer's beta-amyloid precursor protein. J. Neurochem. **60**, 1915-1922

8 Welch, J. E., Brown, P. L., O'Brien, D. A., Magyar, P. L., Bunch, D. O., Mori, C. and Eddy, E. M. (2000) Human glyceraldehyde 3-phosphate dehydrogenase-2 gene is expressed specifically in spermatogenic cells. J. Androl. **21**, 328-338

9 Welch, J. E., Barbee, R. R., Magyar, P. L., Bunch, D. O. and O'Brien, D. A. (2006) Expression of the spermatogenic cell-specific glyceraldehyde 3-phosphate dehydrogenase (GAPDS) in rat testis. Mol. Reprod. Dev. **73**, 1052-1060

10 Westhoff, D. and Kamp, G. (1997) Glyceraldehyde 3-phosphate dehydrogenase is bound to the fibrous sheath of mammalian spermatozoa. J. Cell. Sci. **110 (Pt 15)**, 1821-1829

11 Mukai, C. and Okuno, M. (2004) Glycolysis plays a major role for adenosine triphosphate supplementation in mouse sperm flagellar movement. Biol. Reprod. **71**, 540-547

12 Miki, K., Qu, W., Goulding, E. H., Willis, W. D., Bunch, D. O., Strader, L. F., Perreault, S. D., Eddy, E. M. and O'Brien, D. A. (2004) Glyceraldehyde 3-phosphate dehydrogenase-S, a sperm-specific glycolytic enzyme, is required for sperm motility and male fertility. Proc. Natl. Acad. Sci. U. S. A. **101**, 16501-16506

13 Bone, W. and Cooper, T. G. (2000) In vitro inhibition of rat cauda epididymal sperm glycolytic enzymes by ornidazole, alpha-chlorohydrin and 1-chloro-3-hydroxypropanone. Int. J. Androl. **23**, 284-293

14 Bone, W., Jones, A. R., Morin, C., Nieschlag, E. and Cooper, T. G. (2001) Susceptibility of glycolytic enzyme activity and motility of spermatozoa from rat, mouse, and human to inhibition by proven and putative chlorinated antifertility compounds in vitro. J. Androl. **22**, 464-470

15 Ford, W. C. (2006) Glycolysis and sperm motility: does a spoonful of sugar help the flagellum go round? Hum. Reprod. Update. **12**, 269-274

16 Ford, W. C. and Waites, G. M. (1982) Activities of various 6-chloro-6-deoxysugars and (S) alpha-chlorohydrin in producing spermatocoeles in rats and paralysis in mice and in inhibiting glucose metabolism in bull spermatozoa in vitro. J. Reprod. Fertil. **65**, 177-183

THIS IS NOT THE VERSION OF RECORD - see doi:10.1042/BJ20101442

Accepted Manuscript

Licenced copy. Copying is not permitted, except with prior permission and as allowed by law.
© 2011 The Authors Journal compilation © 2011 Portland Press Limited

Biochemical Journal Immediate Publication. Published on 26 Jan 2011 as manuscript BJ20101442

17 Jelks, K. B. and Miller, M. G. (2001) alpha-Chlorohydrin inhibits glyceraldehyde-3-phosphate dehydrogenase in multiple organs as well as in sperm. Toxicol. Sci. **62**, 115-123
18 Malay, A. D., Bessho, Y., Ellis, M. J., Antonyuk, S. V., Strange, R. W., Hasnain, S. S., Shinkai, A., Padmanabhan, B. and Yokoyama, S. (2009) Structure of glyceraldehyde-3-phosphate dehydrogenase from the archaeal hyperthermophile Methanocaldococcus jannaschii. Acta Crystallogr. Sect. F Struct. Biol. Cryst. Commun. **65**, 1227-1233
19 Yun, M., Park, C. G., Kim, J. Y. and Park, H. W. (2000) Structural analysis of glyceraldehyde 3-phosphate dehydrogenase from Escherichia coli: direct evidence of substrate binding and cofactor-induced conformational changes. Biochemistry. **39**, 10702-10710
20 Castilho, M. S., Pavao, F., Oliva, G., Ladame, S., Willson, M. and Perie, J. (2003) Evidence for the two phosphate binding sites of an analogue of the thioacyl intermediate for the Trypanosoma cruzi glyceraldehyde-3-phosphate dehydrogenase-catalyzed reaction, from its crystal structure. Biochemistry. **42**, 7143-7151
21 Mercer, W. D., Winn, S. I. and Watson, H. C. (1976) Twinning in crystals of human skeletal muscle D-glyceraldehyde-3-phosphate dehydrogenase. J. Mol. Biol. **104**, 277-283
22 Ismail, S. A. and Park, H. W. (2005) Structural analysis of human liver glyceraldehyde-3-phosphate dehydrogenase. Acta Crystallogr. D Biol. Crystallogr. **61**, 1508-1513
23 Jenkins, J. L. and Tanner, J. J. (2006) High-resolution structure of human D-glyceraldehyde-3-phosphate dehydrogenase. Acta Crystallogr. D Biol. Crystallogr. **62**, 290-301
24 Kim, H., Feil, I. K., Verlinde, C. L., Petra, P. H. and Hol, W. G. (1995) Crystal structure of glycosomal glyceraldehyde-3-phosphate dehydrogenase from Leishmania mexicana: implications for structure-based drug design and a new position for the inorganic phosphate binding site. Biochemistry. **34**, 14975-14986
25 Trentham, D. R. (1971) Reactions of D-glyceraldehyde 3-phosphate dehydrogenase facilitated by oxidized nicotinamide-adenine dinucleotide. Biochem. J. **122**, 59-69
26 Michels, S., Rogalska, E. and Branlant, G. (1996) Phosphate-binding sites in phosphorylating glyceraldehyde-3-phosphate dehydrogenase from Bacillus stearothermophilus. Eur. J. Biochem. **235**, 641-647
27 Moniot, S., Bruno, S., Vonrhein, C., Didierjean, C., Boschi-Muller, S., Vas, M., Bricogne, G., Branlant, G., Mozzarelli, A. and Corbier, C. (2008) Trapping of the thioacylglyceraldehyde-3-phosphate dehydrogenase intermediate from Bacillus stearothermophilus. Direct evidence for a flip-flop mechanism. J. Biol. Chem. **283**, 21693-21702
28 Ryzlak, M. T. and Pietruszko, R. (1988) Heterogeneity of glyceraldehyde-3-phosphate dehydrogenase from human brain. Biochim. Biophys. Acta. **954**, 309-324
29 Frayne, J., Taylor, A., Cameron, G. and Hadfield, A. T. (2009) Structure of insoluble rat sperm glyceraldehyde-3-phosphate dehydrogenase (GAPDH) via heterotetramer formation with Escherichia coli GAPDH reveals target for contraceptive design. J. Biol. Chem. **284**, 22703-22712
30 CCP4. (1994) The CCP4 suite: programs for protein crystallography. Acta Crystallogr. D Biol. Crystallogr. **50**, 760-763
31 McCoy, A. J., Grosse-Kunstleve, R. W., Storoni, L. C. and Read, R. J. (2005) Likelihood-enhanced fast translation functions. Acta Crystallogr. D Biol. Crystallogr. **61**, 458-464
32 Cowtan, K. (1999) Error estimation and bias correction in phase-improvement calculations. Acta Crystallogr. D Biol. Crystallogr. **55**, 1555-1567
33 Cowtan, K. (2006) The Buccaneer software for automated model building. 1. Tracing protein chains. Acta Crystallogr. D Biol. Crystallogr. **62**, 1002-1011
34 Emsley, P. and Cowtan, K. (2004) Coot: model-building tools for molecular graphics. Acta Crystallogr. D Biol. Crystallogr. **60**, 2126-2132

THIS IS NOT THE VERSION OF RECORD - see doi:10.1042/BJ20101442
Accepted Manuscript
Licenced copy. Copying is not permitted, except with prior permission and as allowed by law.
© 2011 The Authors Journal compilation © 2011 Portland Press Limited

Biochemical Journal Immediate Publication. Published on 26 Jan 2011 as manuscript BJ20101442

35 Murshudov, G. N., Vagin, A. A. and Dodson, E. J. (1997) Refinement of macromolecular structures by the maximum-likelihood method. Acta Crystallogr. D Biol. Crystallogr. **53**, 240-255
36 Painter, J. and Merritt, E. A. (2006) Optimal description of a protein structure in terms of multiple groups undergoing TLS motion. Acta Crystallogr. D Biol. Crystallogr. **62**, 439-450
37 Ferdinand, W. (1964) The isolation and specific activity of rabbit-muscle glyceraldehyde phosphate dehydrogenase. Biochem. J. **92**, 578-585
38 Buehner, M., Ford, G. C., Moras, D., Olsen, K. W. and Rossmann, M. G. (1974) Structure determination of crystalline lobster D-glyceraldehyde-3-phosphate dehydrogenase. J. Mol. Biol. **82**, 563-585
39 Olsen, K. W. (1983) Structural basis for the thermal stability of glyceraldehyde-3-phosphate dehydrogenases. Int. J. Pept. Protein Res. **22**, 469-475
40 Didierjean, C., Corbier, C., Fatih, M., Favier, F., Boschi-Muller, S., Branlant, G. and Aubry, A. (2003) Crystal structure of two ternary complexes of phosphorylating glyceraldehyde-3-phosphate dehydrogenase from Bacillus stearothermophilus with NAD and D-glyceraldehyde 3-phosphate. J. Biol. Chem. **278**, 12968-12976
41 Elkina, Y. L., Kuravsky, M. L., El'darov, M. A., Stogov, S. V., Muronetz, V. I. and Schmalhausen, E. V. (2010) Recombinant human sperm-specific glyceraldehyde-3-phosphate dehydrogenase: structural basis for enhanced stability. Biochim. Biophys. Acta. **1804**, 2207-2212
42 Kochman, M., Golebiowska, J., Baranowski, T., Dedman, J. R., Fodge, D. W. and Harris, B. G. (1974) Hybridization of glyceraldehyde-3-phosphate dehydrogenase. FEBS Lett. **41**, 104-107
43 Li, L., Luo, M., Ghanem, M., Taylor, E. A. and Schramm, V. L. (2008) Second-sphere amino acids contribute to transition-state structure in bovine purine nucleoside phosphorylase. Biochemistry. **47**, 2577-2583
44 Read, J. A., Winter, V. J., Eszes, C. M., Sessions, R. B. and Brady, R. L. (2001) Structural basis for altered activity of M- and H-isozyme forms of human lactate dehydrogenase. Proteins. **43**, 175-185
45 Trentham, D. R., McMurray, C. H. and Pogson, C. I. (1969) The active chemical state of D-glyceraldehyde 3-phosphate in its reactions with D-glyceraldehyde 3-phosphate dehydrogenase, aldolase and triose phosphate isomerase. Biochem. J. **114**, 19-24
46 Baker, N. A., Sept, D., Joseph, S., Holst, M. J. and McCammon, J. A. (2001) Electrostatics of nanosystems: application to microtubules and the ribosome. Proc. Natl. Acad. Sci. U. S. A. **98**, 10037-10041

THIS IS NOT THE VERSION OF RECORD - see doi:10.1042/BJ20101442

Accepted Manuscript

Licenced copy. Copying is not permitted, except with prior permission and as allowed by law.
© 2011 The Authors Journal compilation © 2011 Portland Press Limited

Biochemical Journal Immediate Publication. Published on 26 Jan 2011 as manuscript BJ20101442

TABLES

Table 1 Data Collection and Refinement Statistics for hGAPDS$_{\Delta N}$ structures

Complex	**hGAPDS$_{\Delta N}$-NAD$^+$-PO$_4$**	**hGAPDS$_{\Delta N}$-NAD$^+$-GOL**
PDB id	3h9e	3pfw
Data collection		
Beamline	Diamond Light Source, I03	Rigaku FR-E Superbright
Wavelength (Å)	0.9763	1.5418
Spacegroup	*C*2	*C*2
Resolution range[a] (Å)	68.23 – 1.72 (1.81 – 1.72)	23.49 – 2.15 (2.27-2.15)
Unit cell dimensions	*a* = 142.0, *b* = 71.8, *c* = 81.3 Å α = γ = 90.0°, β = 122.9°	*a* = 143.6, *b* = 71.9, *c* = 81.1 Å α = γ = 90.0°, β = 123.3°
No. unique reflections[a]	72,227 (10,230)	35,308 (5,001)
Completeness[a] (%)	99.2 (96.3)	94.1 (92.0)
I/σI[a]	11.4 (2.3)	7.0 (2.3)
R_{merge}[a] (%)	7.7 (51.4)	17.1 (67.1)
Redundancy[a]	4.4 (3.6)	5.3 (5.3)
Refinement		
No. atoms in refinement (P/L/O)[b]	5301/ 108/ 523	5194/ 124/ 310
R_{cryst} (%)	14.3	16.8
R_{free} (%)	17.6	22.2
B-factor (P/L/O)[b] (Å^2)	26/ 20/ 29	28/ 32/ 30
RMSD bond length[c] (Å)	0.014	0.016
RMSD bond angle[c] (°)	1.50	1.54
Ramadrandran plot		
Favoured region	97.0	95.9
Allowed region	99.7	99.7

[a] Values in brackets show the statistics for the highest resolution shells.
[b] P/L/O denote protein, active-site ligands and other solvent molecules, respectively
[c] RMSD, root-mean-square deviation.

THIS IS NOT THE VERSION OF RECORD - see doi:10.1042/BJ20101442

Accepted Manuscript

Licenced copy. Copying is not permitted, except with prior permission and as allowed by law.
© 2011 The Authors Journal compilation © 2011 Portland Press Limited

Table 2 Steady-state kinetic properties hGAPDS$_{\Delta N}$ and hGAPDH.

	hGAPDS$_{\Delta N}$	hGAPDH
K_M NAD^+ (μM)	35 ± 8	100 ± 38
K_M D-G3P (mM)	0.46 ± 0.18* (0.037)**	0.25 ± 0.09* (0.020)**
k_{cat} (s^{-1})	234 ± 24	199 ± 17
V_{max} (μmole/min/mg)	405 ± 41	340 ± 31

Calculations of K_M for D-G3P were based either on *an assumption of an equal concentration of D- and L-G3P in the racemic DL-G3P, or **an approximate 4% D-G3P as the active aldehyde in the racemic substrate according to [45], however the latter is not considered in other GAPDH kinetic analyses.

THIS IS NOT THE VERSION OF RECORD - see doi:10.1042/BJ20101442

Accepted Manuscript

Licenced copy. Copying is not permitted, except with prior permission and as allowed by law.
© 2011 The Authors Journal compilation © 2011 Portland Press Limited

Biochemical Journal Immediate Publication. Published on 26 Jan 2011 as manuscript BJ20101442

THIS IS NOT THE VERSION OF RECORD - see doi:10.1042/BJ20101442

FIGURE LEGENDS

Figure 1 Structural overview, surface electrostatic potentials and selectivity cleft of hGAPDS$_{\Delta N}$. (**A**) The asymmetric unit of hGAPDS$_{\Delta N}$-NAD$^+$-PO$_4$ complex comprises subunits *O* and *P*, each composed of the N- (green) and C-domains (cyan) (*inset*). (**B**) The hGAPDS$_{\Delta N}$ homo-tetramer is assembled from the *OP* dimer and the *QR* dimer generated by a two-fold crystallographic symmetry operator (grey plane) lying on the *RQ* plane. (**C**) Surface electrostatic potentials of hGAPDS$_{\Delta N}$ calculated by APBS program [46] reveal three prominently charged regions: the negatively-charged S-loop (blue), positively-charged 350-372 region (red) and mix-charged 110-130 region (orange). The *inset* shows calculated electrostatic potentials for somatic hGAPDH (PDB id 1u8f). (**D**) Superposition of the hGAPDS$_{\Delta N}$ selectivity cleft in closed conformation (yellow backbone) with two structures of somatic hGAPDHs showing the closed (blue, PDB id 1u8f) and open conformations (orange, PDB id 1znq). The closed conformation in hGAPDS is stabilized by water-mediated hydrogen bonds (blue dashed lines, water in yellow sphere), similar to that seen in hGAPDH (green dashed lines, water in blue spheres). (**E**) Space-filling representation of the hGAPDS$_{\Delta N}$ selectivity cleft (yellow) reveals a much reduced cavity than *Lm*GAPDH (magenta, PDB id 1i32) due to the bulky Phe108, Pro263 and Arg265. The trypanosomal GAPDH inhibitor NMDBA (orange) is modelled into the hGAPDS structure based on the binding position of the adenine ring of the NAD$^+$ cofactor and illustrates several clashes between the ligand and the protein.

Figure 2 Phosphate binding sites in hGAPDS$_{\Delta N}$. (**A**) Refined 2F_o-F_c map (contoured at 1.0 σ) for NAD$_+$ and phosphate ions in the hGAPDS$_{\Delta N}$-NAD$_+$-PO$_4$ complex. (**B**) Superposition of phosphate-bound *Lm*GAPDH (semi-transparent '*lm*', PDB id 1gyp) and sulphate-bound *Bs*GAPDH (semi-transparent '*bs*', PDB id 1gd1) onto hGAPDS$_{\Delta N}$-NAD$_+$-PO$_4$ subunit *O* (grey) maps the two bound phosphates in hGAPDS$_{\Delta N}$ (grey sticks) at the P$_s$ site, and at the new P$_i$ site. The positions of the original and new P$_i$ sites identified from various GAPDH structures are shown. (**C**) Interactions of phosphates at the P$_s$ (*left*) and new P$_i$ (*right*) sites. Note that at the new P$_i$ site, the closest phosphate oxygen atom is 3.3 Å away from the Cys244 thiol group. (**D**) Two conformations of the active site segment in hGAPDS$_{\Delta N}$-NAD$_+$-PO$_4$ complex: an 'in' conformation in subunit *O* (*left*), and mixed 'in' (semi-transparent)-'out' (grey) conformations in subunit *P* (*right*).

Figure 3 Glycerol binding in the hGAPDS$_{\Delta N}$-NAD$^+$-Gol complex. (**A**) *Left*, F_o-F_c difference density in the active site of both subunits (contoured at 3σ) was modelled as glycerol. *Right,* Phosphate anions from the hGAPDS$_{\Delta N}$-NAD$_+$-PO$_4$ structure (semi-transparent), and two D-G3P molecules (dotted transparent) one bound at the P$_s$ site ('*rs*', from rat GAPDS-NAD$^+$-G3P complex, PDB id 2vyv) and the other at the P$_i$ site ('*lm*', from *Lm*GAPDH-NAD$^+$-G3P complex, PDB id 3cmc) are overlaid. (**B**) Interactions of the two glycerol molecules (Gol) in subunits *O* (*top*) and *P* (*bottom*) of hGAPDS$_{\Delta N}$. Water molecules are represented as blue spheres, and hydrogen bond networks as dashed lines. Note the water-mediated hydrogen bond network bridging the two glycerol molecules is highly conserved among various binding conformations of glycerol.

Figure 4 Amino acid substitutions peripheral to the active sites between hGAPDS$_{\Delta N}$ and hGAPDH. (**A**) Amino acid differences between hGAPDS$_{\Delta N}$ and hGAPDH are clustered in two regions of the active site: one adjacent to the adenine binding pocket and the other at the nicotinamide binding pocket. Residue labels are coloured blue (basic), red (acidic), green (uncharged polar) or grey (non-polar). (**B**) Moderate differences in electrostatic potentials of the cofactor pocket and catalytic pocket between hGAPDS$_{\Delta N}$ and hGAPDH are circled.

Accepted Manuscript

Licenced copy. Copying is not permitted, except with prior permission and as allowed by law.
© 2011 The Authors Journal compilation © 2011 Portland Press Limited

THIS IS NOT THE VERSION OF RECORD - see doi:10.1042/BJ20101442

Figure 1

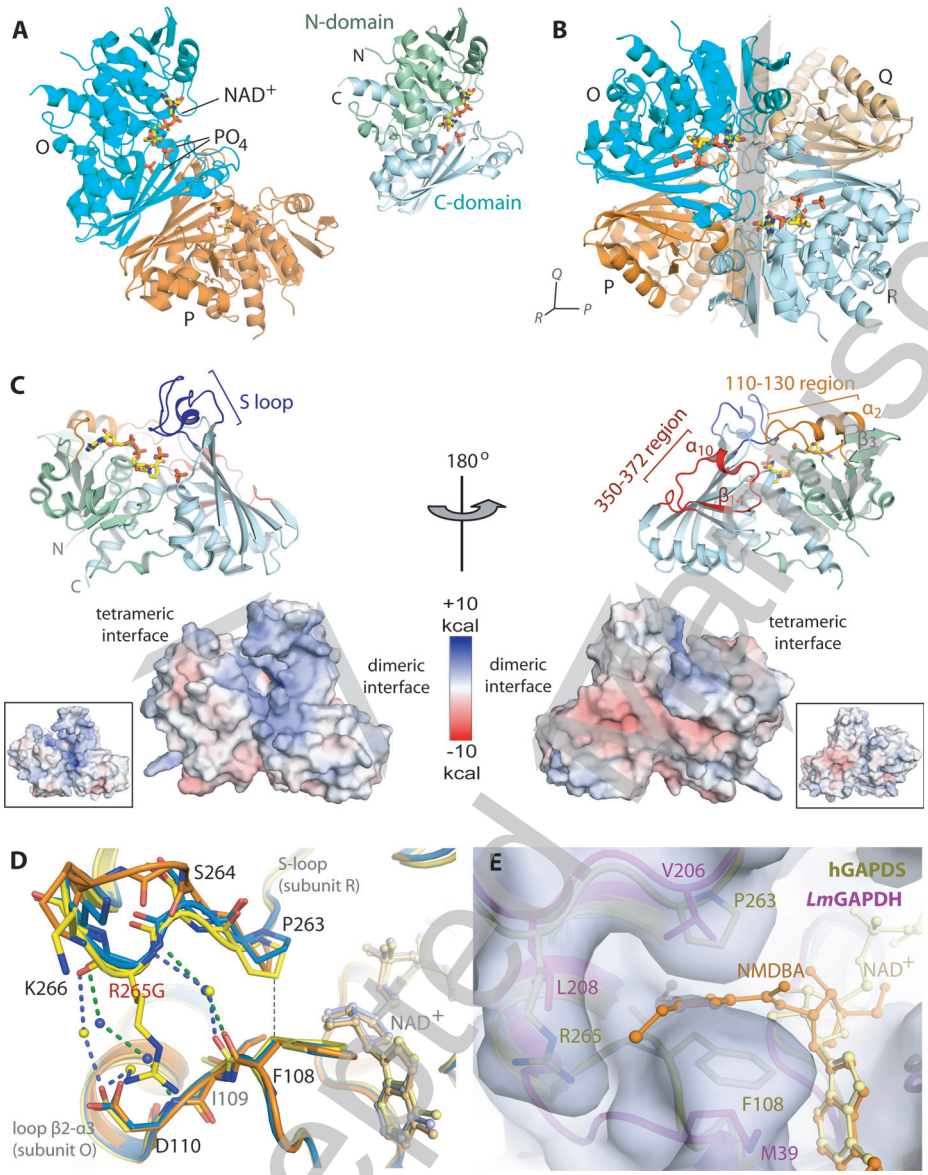

Accepted Manuscript

Licenced copy. Copying is not permitted, except with prior permission and as allowed by law.
© 2011 The Authors Journal compilation © 2011 Portland Press Limited

THIS IS NOT THE VERSION OF RECORD - see doi:10.1042/BJ20101442

Figure 2

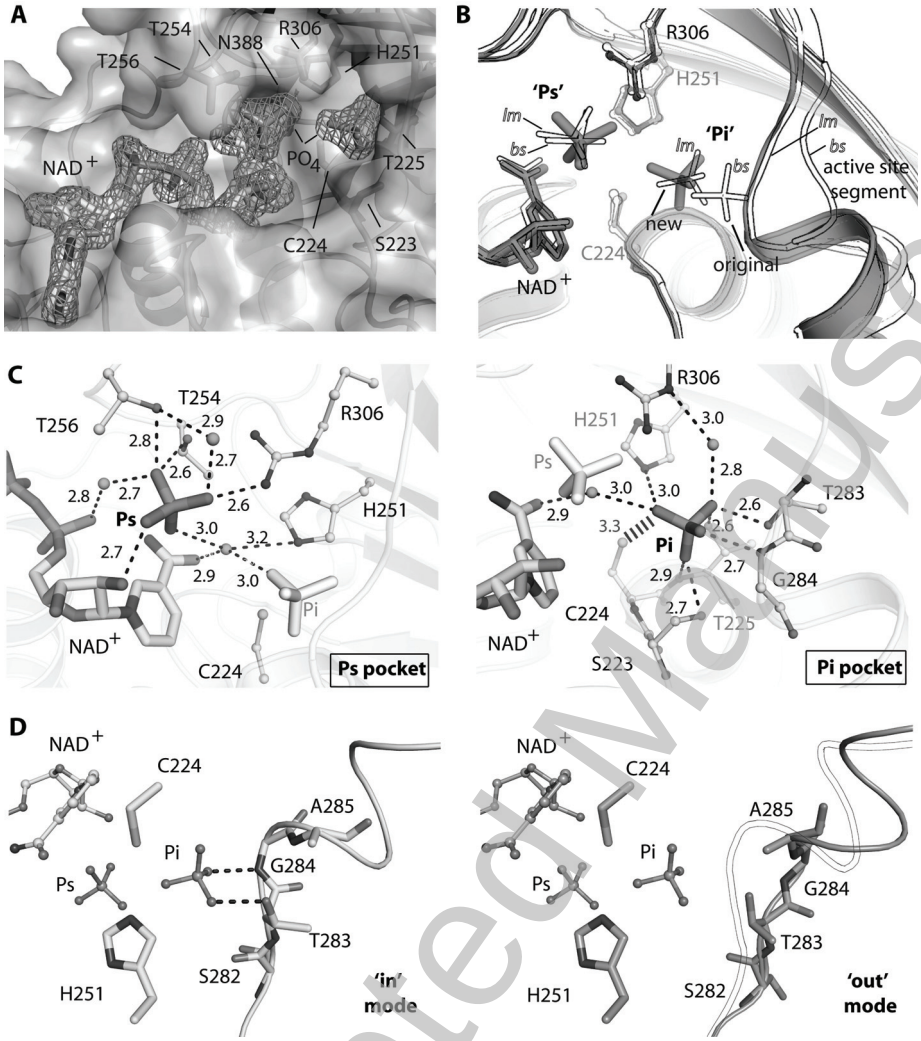

Accepted Manuscript

Licenced copy. Copying is not permitted, except with prior permission and as allowed by law.
© 2011 The Authors Journal compilation © 2011 Portland Press Limited

Figure 3

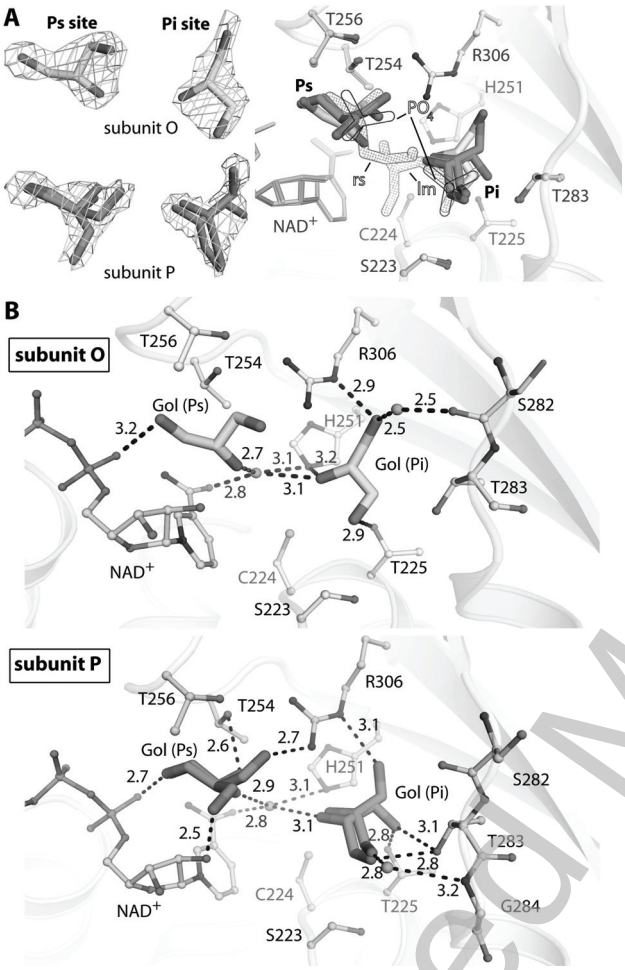

THIS IS NOT THE VERSION OF RECORD - see doi:10.1042/BJ20101442

Accepted Manuscript

Licenced copy. Copying is not permitted, except with prior permission and as allowed by law.
© 2011 The Authors Journal compilation © 2011 Portland Press Limited

Figure 4

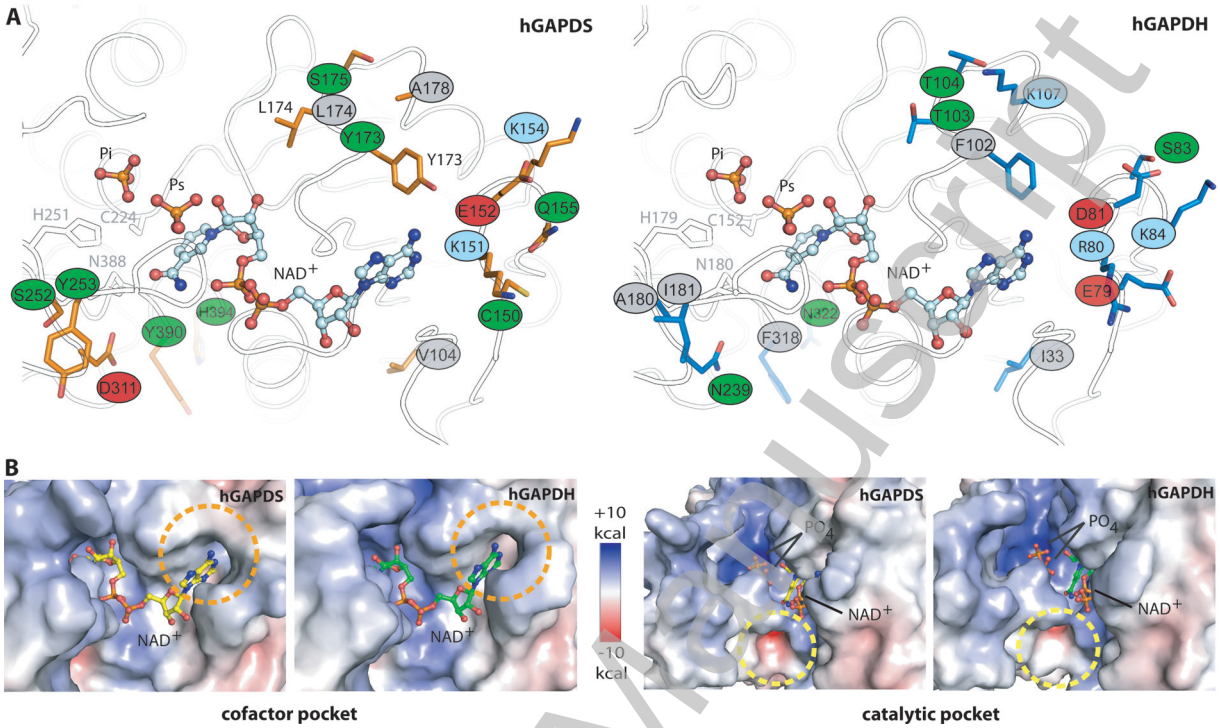

THIS IS NOT THE VERSION OF RECORD - see doi:10.1042/BJ20101442

Accepted Manuscript

Licenced copy. Copying is not permitted, except with prior permission and as allowed by law.
© 2011 The Authors Journal compilation © 2011 Portland Press Limited